Nonlinearity 4 (1991) 1159–1182. Printed in the UK

Bifocal homoclinic orbits in four dimensions

A C Fowler† and C T Sparrow‡

†Mathematical Institute, University of Oxford, 24–29 St Giles', Oxford OX1 3LB, UK

‡Department of Pure Mathematics and Statistics, University of Cambridge, 16 Mill Lane, Cambridge CB2 1SB, UK

Received 19 October 1990, in final form 6 March 1991

Accepted by J D Gibbon

Abstract. We study the bifurcations which occur as we perturb four-dimensional systems of ordinary differential equations having homoclinic orbits that are bi-asymptotic to a fixed point with a double-focus structure. We give several methods of understanding the geometry of the invariant set that exists close to the homoclinic orbit and introduce a multi-valued one-dimensional map which can be used to predict the behaviour and bifurcation patterns which may occur. We argue that, although local strange behaviour is likely to occur, in a global sense (i.e. for large enough perturbations) the whole sequence of bifurcations produces a single periodic orbit, just as in the three-dimensional saddle-focus case.

AMS classification scheme numbers: 34A34, 34C35, 58F13

1. Introduction

Many features of chaotic behaviour in ordinary differential equations can be understood by the analysis of homoclinic bifurcations associated with homoclinic orbits which are bi-asymptotic (as $t \to \pm\infty$) to a fixed point of the flow. This point of view was advanced by Sparrow (1982) in analysing the Lorenz equations, and also by Glendinning and Sparrow (1984), Arneodo *et al.* (1982), Tresser (1984), and Gaspard (1984) in extending Shil'nikov's pioneering work (1965, 1970) on systems with a homoclinic orbit to a saddle-focus.

The idea of such an analysis is that one approximates a Poincaré map for a flow by approximating trajectories which are sufficiently close to the homoclinic orbit, and that one then studies this map to deduce facts about the dynamics of the flow. To be specific, consider the differential equation

$$\dot{x} = f(x, \mu), \qquad x \in \mathbb{R}^n \tag{1.1}$$

where μ is a parameter. We assume that when $\mu = 0$, there is a homoclinic orbit $\Gamma = \{x_0(t), -\infty < t < \infty, x_0(0) \neq 0, x_0(t) \to 0 \text{ as } t \to \pm\infty\}$ biasymptotic to a fixed point at $x = 0$. For μ small we choose a 'box' $B: |x| \leqslant c$, where $c \ll 1$, and take one 'face' of it, S, as the Poincaré surface. Suppose that Γ leaves B through a face S' at a point

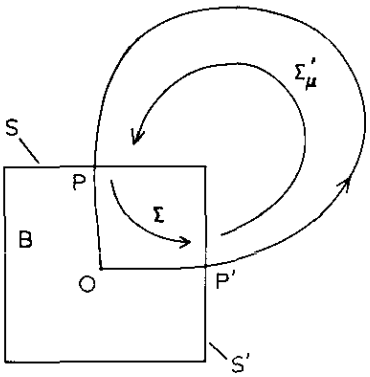

Figure 1. The sets S and S' and the maps Σ and Σ'_μ.

P' and re-enters through S at a point P (see figure 1). For x within B we have

$$\dot{x} = Df(0, \mu)x + O(|x^2|) \tag{1.2}$$

and the flow is approximately linear. Hence, using (1.2), we can calculate an approximate map, Σ, from S to S'. Outside B, if a trajectory starts on S' near P' we can write

$$x(t) = x_0(t) + y(t) \qquad \dot{y} = Df[x_0(t), \mu]y + O(y^2)$$

and, in principle, solve this equation to find the point where $x(t)$ enters B close to P on S. Providing both μ and the initial y are small compared with c, and that the time spent going from S' to S is small relative to the time spent by a trajectory in B, we can approximate the map from S to S' by an equation of the form Σ'_μ: $S' \to S$,

$$\Sigma'_\mu(x) = P + \mu e + A(x - P') + O(y^2, \mu^2, \mu y) \tag{1.3}$$

where A is a non-singular $(n-1) \times (n-1)$ matrix with entries which depend on the details of the global flow outside B, and e is a vector determined by how the global flow changes with μ.

Composition of the two maps Σ and Σ'_μ then gives a mapping from S back to S. This will be highly nonlinear due to the distortion near O.

For this analysis to be valid, we require that $\mu \ll c$, and that we only consider trajectories which spend a long time in B. It follows from this that in their passage through B, the more stable eigencomponents of x are exponentially reduced relative to the least stable eigencomponents; for similar reasons, only those elements in S with exponentially small unstable eigencomponents relative to the least unstable will emerge through S' close enough to Γ to hit S again on the next pass. The implication of this is that the Poincaré map can be approximately taken from consideration only of the eigencomponents with eigenvalues nearest to zero. These ideas were used by Neimark and Shil'nikov (1965) and Shil'nikov (1968) in analysing near-homoclinic behaviour in n dimensions.

In consequence, there are three main types of homoclinic bifurcation (from a fixed point). These are where the least stable and unstable eigenvalues are (i) both real; (ii) one real, one complex pair; (iii) two complex pairs. Case (i) is uninteresting, unless a symmetry is present. (One of the possible symmetries gives the Lorenz case (Sparrow 1982) when the expanding eigenvalue is of greater absolute magnitude than the relevant contracting eigenvalue.) Case (ii) is that of

Shil'nikov (1965), which has been extensively studied (see below). Case (iii) has also been studied by Shil'nikov (1967, 1970), and is our subject here.

Shil'nikov's early results were as follows: he showed (1965) that in case (ii) above, when $\mu = 0$ and $n = 3$ in (1.1), there may exist a countable number of periodic orbits. Later (1967), he obtained the same result in case (iii) (at $\mu = 0$, $n = 4$). This analysis was extended to n dimensions and $\mu \neq 0$ (Neimark and Shil'nikov 1965, Shil'nikov 1968), but only in obtaining criteria for the bifurcation of a single periodic orbit. Later (1970), Shil'nikov extended the analysis of cases (ii) and (iii) to n dimensions, to obtain (via symbolic dynamics) the result that at $\mu = 0$, there exist uncountably many aperiodic orbits. The major achievement of Glendinning and Sparrow (1984) and Gaspard (1984) was to show that the bifurcations associated with case (ii) when $\mu \neq 0$, and when countably many periodic solutions exist at $\mu = 0$, could be viewed in terms of the existence of a one parameter family of periodic solutions, which exist in a neighbourhood of $\mu = 0$, and whose period P is determined implicitly by $\mu = \mu(P)$, where $\mu(P)$ is single-valued but not (necessarily) monotonic. Thus Shil'nikov's (1965) result was extended to $\mu \neq 0$, and by Gaspard (1984) also to n dimensions.

In this paper, we extend the methods of analysis of Glendinning and Sparrow (1984) to case (iii) above, where there exists, at a value $\mu = 0$, an orbit homoclinic to a fixed point of double-focus (bifocal) type. We specifically consider $n = 4$ (but expect our results to apply in general if $n > 4$) and $\mu \neq 0$. We begin by deriving an approximate Poincaré map from a subset of $\mathbb{R}^3$ into $\mathbb{R}^3$, and we show that this map is naturally defined on a small part of a torus. In seeking to determine the invariant set of this Poincaré map, we then show that this set is contained in a neighbourhood of a spiral sheet (shaped like a *scroll*); then the invariant set is in fact a neighbourhood of the intersection of this scroll and its image under the map, which we show to be another scroll, in general skewed and offset from the original.

The following parts of the paper establish the topological nature of the constituents of the scroll intersections, and elucidate how the components evolve as the parameter μ varies. We give a variety of ways of describing both the geometry of the components, and the dynamics of the map on them. In particular, we show that the Poincaré map *on the invariant set* is close to a multi-valued one-dimensional map, whose multi-valuedness stems from the ability of the real (3D) Poincaré map to transfer between different components of the invariant set, and we use this one-dimensional map to infer results on periodic orbits. For example, we show that there is a one-parameter family of (primary) periodic orbits whose period P is determined implicitly via $\mu = \mu(P)$; we give explicit formulae for $\mu(P)$, which are analogous to the three-dimensional Shil'nikov case. Finally, we point out some novel bifurcations which may occur in examples of this sort.

There are two standard ways of proving the various Shil'nikov theorems and making rigorous our derivation of the maps Σ and Σ'_μ above. One way, following Tresser (1984) is the following. By the Hartman–Grobman theorem (Hartman 1982), the local flow near 0 determined by (1.2) is homeomorphic to the linear flow of ξ satisfying

$$\dot{\xi} = Df(0, \mu)\xi. \tag{1.4}$$

The homeomorphism will in fact be a diffeomorphism (i.e. smooth), provided certain non-resonance conditions among the eigenvalues of $Df(0, \mu)$ are satisfied

(Hartman 1982, Belitskii 1978). In this case, we can smoothly linearize the flow near 0, and by an extension, we obtain a global flow which is linear in a neighbourhood of 0. Then the approximate Poincaré map is constructed as outlined, and is close to the actual map. The existence of fixed points follows from the use of the implicit function theorem, and the use of symbolic dynamics applied to embedded Smale horseshoes leads to the aperiodic orbits (see also Guckenheimer and Holmes (1983)).

Shil'nikov (and Gaspard), using the other technique, avoid the problem of resonant eigenvalues by rewriting the flow (1.2) as an integral equation for x, and invoking standard smoothness theorems on the solution. The remainder of this proof then follows Tresser's outline. The recent book by Wiggins (1988) contains detailed discussion concerning the proof of results obtained from these kinds of analysis.

In this paper we will avoid all such technical issues and concentrate on analysing the appropriate return map which we obtain in section 2 by the technique described at the beginning of this section. Our aims are to understand the geometry of the invariant set for small μ and the way in which it bifurcates as μ changes (section 3), to compute a multi-valued one-dimensional map which can be used to predict the behaviour of trajectories and sequences of bifurcations (section 4), and to sketch a proof of a theorem that there is a one-parameter family of periodic orbits in a neighbourhood of Γ, for small $\mu \neq 0$, with period P related to μ via a single-valued function $\mu(P)$, which has an infinite number of zeros which accumulate at $P = \infty$ (section 5). We shall also argue that our results imply that the global effect of the homoclinic bifurcation (if we look outside a large enough neighbourhood of $\mu = 0$) is to produce a single periodic orbit, just as in the three-dimensional saddle-focus case (Glendinning and Sparrow 1984). In the course of the analysis, we shall indicate reasons why and how various other 'typical' behaviours may be expected, such as period-doubling and subsidiary homoclinic orbits. Our discussion will be discursive, but will, we hope, provide methods for understanding behaviour likely to be observed in examples.

2. A Poincaré map for the bifocal case

The derivation of a Poincaré map for a four-dimensional system with a homoclinic orbit proceeds analogously to that for two- and three-dimensional systems, as expounded, for example, by Sparrow (1982) and Glendinning and Sparrow (1984) and as explained above. The flow in the neighbourhood of a homoclinic orbit (which we assume exists when a parameter $\mu = 0$) consists of two parts; firstly, when the trajectory is near the fixed point, the behaviour is essentially described by the linearized equations of the system about the fixed point. Secondly, away from the origin, the nonlinear equations can be linearized about the homoclinic orbit. Hence a Poincaré map for nearly homoclinic trajectories can be constructed analytically, which is valid to arbitrary accuracy as μ (the bifurcation parameter) becomes small.

Let us first suppose the fixed point with which we are concerned to be the origin, and consider the flow in a small neighbourhood of the origin. We define local polar coordinates $(r_1, \theta_1, r_2, \theta_2)$. The linear behaviour near the origin can be represented

as:

$$\begin{aligned} \dot{r}_1 &= -\lambda_1 r_1 \\ \dot{\theta} &= \omega_1 \\ \dot{r}_2 &= \lambda_2 r_2 \\ \dot{\theta}_2 &= \omega_2 \end{aligned} \tag{2.1}$$

where we take $\lambda_1, \lambda_2 > 0$. The set of equations (2.1) represents the assumption that the origin is a double focus. We will assume that λ_1, λ_2, ω_1 and ω_2 are independent of μ, though more generally that would not be the case. This assumption simplifies our formulae without affecting the results of the analysis. To construct a Poincaré map, we consider a three-dimensional return surface S, which is the interior of a torus near the origin defined by:

$$S: r_1 = h \qquad 0 \leqslant \theta_1, \ \theta_2 \leqslant 2\pi \qquad 0 \leqslant r_2 \leqslant \bar{r}_2. \tag{2.2}$$

Here h is small, as is $\bar{r}_2$. While r_1 and r_2 are small, we follow points initially in S through to another torus S', defined by:

$$S': r_2 = k \qquad 0 \leqslant \theta_1, \ \theta_2 \leqslant 2\pi \qquad 0 \leqslant r_1 \leqslant \bar{r}_1. \tag{2.3}$$

Again, k is small. By solving (2.1) we find that a point $(r_2^0, \theta_1^0, \theta_2^0)$ in S is mapped to a point $(r_1', \theta_1', \theta_2')$ in S', given by:

$$\begin{aligned} r_1' &= h[k/r_2^0]^{-\lambda_1/\lambda_2} \\ \theta_1' &= \theta_1^0 + \frac{\omega_1}{\lambda_2} \ln[k/r_2^0] \\ \theta_2' &= \theta_2^0 + \frac{\omega_2}{\lambda_2} \ln[k/r_2^0]. \end{aligned} \tag{2.4}$$

Following the notation introduced in the previous section, we call this map $\Sigma: S \to S'$. Evidently, we can take $\bar{r}_1 = h(k/\bar{r}_2)^{-\lambda_1/\lambda_2}$ in (2.3) since this gives us a sufficiently large torus S' that any trajectory started in S which does not tend to the origin will leave the neighbourhood of the origin through S'. Notice that θ_1 is the axial angle in S, whereas θ_2 is the axial angle in S', so that the angle variables are interchanged in going from S to S' (this reflects an extremely complex behaviour of the map Σ, as we see below). See also figure 2.

Next we calculate a map Σ_μ' from S' to S determined by the global flow. The circle $r_2 = 0$ in S is in the stable manifold of the origin 0. The circle $r_1 = 0$ in S' is in the unstable manifold of 0. By assumption there is (when $\mu = 0$) a point P' on $r_1 = 0$ in S' which maps through the flow along the homoclinic orbit into a point P on $r_2 = 0$ in S. We can define the origins of θ_2 in S and θ_1 in S', so that P satisfies $\theta_2 = 0$, and P' satisfies $\theta_1 = 0$.

Under the flow, the solid torus S' is mapped near to S by Σ_μ'. For sufficiently small μ, $\Sigma_\mu'(P')$ is close to P, and thus $\Sigma_\mu'(S') \cap S$ will be non-empty. However, as can be seen from figure 2, most points in $\Sigma_\mu'(S')$ do not intersect S. We only wish to consider those points in S which return to S under Σ and Σ_μ', and those which do are those which have images under Σ close to P' in S'. For such points the map Σ_μ' may be linearised as a first approximation. Evidently, this requires $\mu \ll h, k$ (i.e. take S and S' sufficiently far from the origin), and we thus restrict our attention to the

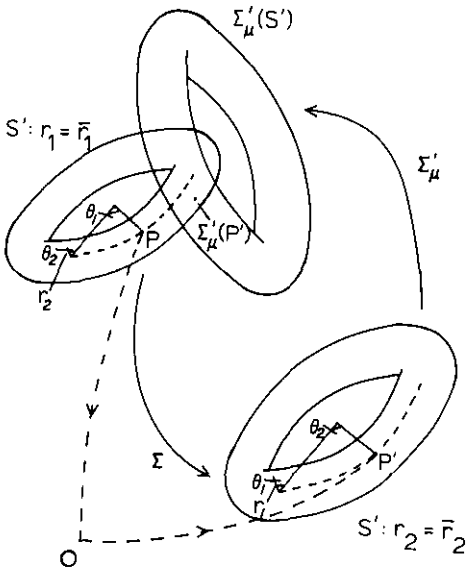

Figure 2. When $\mu = 0$, $\Sigma'_\mu(P')$ coincides with P. However, for all small μ, most of $\Sigma'_\mu(S')$ does not intersect S.

values of θ_2 in S' satisfying $|\theta_2| \ll 1$ which will map into S. Now define local cartesian coordinates:

$$\begin{aligned} X' &= r'_1 \cos\theta'_1 \\ Y' &= r'_1 \sin\theta'_1 \qquad \text{in } S' \\ Z' &= k\theta'_2 \\ X &= r^1_2 \cos\theta^1_2 \\ Y &= r^1_2 \sin\theta^1_2 \qquad \text{in } S. \\ Z &= h\theta_1 \end{aligned} \tag{2.5}$$

The flow near the homoclinic orbit then maps S' to S via the approximation $\Sigma'_\mu: S' \to S$ defined by the affine transformation

$$\begin{pmatrix} X \\ Y \\ Z \end{pmatrix} = \begin{pmatrix} r^1_2 \cos\theta^1_2 \\ r^1_3 \sin\theta^1_2 \\ Z \end{pmatrix} = A \begin{pmatrix} r'_1 \cos\theta'_1 \\ r'_1 \sin\theta'_1 \\ Z' \end{pmatrix} + \mathbf{d}\mu. \tag{2.6}$$

The matrix A is invertible. Composition of (2.4) and (2.6) defines a *Poincaré map* $\varphi: S \to S$ which takes $(r^0_2, \theta^0_1, \theta^0_2)$ to $(r^1_2, \theta^1_1, \theta^1_2)$ via a point $(r'_1, \theta'_1, \theta'_2)$ in S'. φ is only defined for points in S which make it back to S, and as already mentioned, these are points such that θ_2 is small in S', and also (with the same argument) such that θ^0_1 is small in S.

We are therefore led to consider a small part of S, $S_0 \subset S$, defined by

$$S_0: r_1 = h \qquad r_2 \leqslant \bar{r}_2 \qquad |\theta_1| \leqslant \varepsilon_1 \qquad \left|\theta_2 + \frac{\omega_2}{\lambda_2} \ln\left(\frac{k}{r_2}\right)\right| \leqslant \varepsilon_2. \tag{2.7}$$

The second inequality restricts attention to the part of S near to P, whilst the third ensures that the image under Σ in S' is near to P'. This image, $\Sigma(S_0) = S'_0$, is given

from (2.4) by

$$S_0': r_1 \leqslant h\left(\frac{\bar{r}_2}{k}\right)^{\delta} \qquad r_2 = k \qquad \left|\theta_1 - \frac{\omega_1}{\lambda_1}\ln\left(\frac{h}{r_1}\right)\right| \leqslant \varepsilon_1 \qquad |\theta_2| \leqslant \varepsilon_2 \tag{2.8}$$

with $\delta = \lambda_1/\lambda_2$.

Both (2.7) and (2.8) define three-dimensional sets which, if we choose ε_1 and ε_2 small (see below) lie close to two-dimensional sets with the form of a cylindrical logarithmic spiral. A representation of the set S_0 is shown in figure 3. We will refer to S_0 as a spiral sheet, or *scroll*. When we need to emphasize its three-dimensionality, we will call it a *thick scroll*.

We shall speak of the *width* of S_0 as its extent in the axial (Z) direction which is, in this case, $h\varepsilon_1$. The *relative thickness* we define as the (relative) extent in the radial direction.

At constant θ_2, points on opposite sides of S_0 have $\ln(r_2^+/r_2^-) \sim O(\varepsilon_2)$ from (2.7), where $r_2^{\pm}$ are r_2 values on the outer and inner sides respectively. Hence

$$\frac{\Delta r_2}{r_2} \sim O(\varepsilon_2) \tag{2.9}$$

where $\Delta r_2 = r_2^+ - r_2^-$ is the actual radial thickness and $\Delta r_2/r_2$ is the relative radial thickness. Similar definitions apply to S_0', which has width measured by $Z' = k\varepsilon_2$ and relative thickness $\Delta r_1/r_1 \sim O(\varepsilon_1)$. Notice that the transformation of the spiral S_0 to the spiral S_0' is extremely complicated since the θ_1 and θ_2 directions are interchanged. This reflects an enormous stretching (in the θ_2 direction) and contraction (in the θ_1 direction) which are two of the hallmarks of horseshoes in the map. (These statements are justified below.)

The other part of the Poincaré map Σ_μ' which takes S' to S, is simply the affine transformation (2.6). This may disturb the scroll S_0' by rotation, magnification, etc., but the image $\Sigma_\mu'(S_0') = \varphi(S_0)$ will still be a thick scroll which is almost two-dimensional. In general, the scroll $\varphi(S_0)$ will have its axis displaced from that of S and skew to it as indicated in figure 4 (the axes intersect at P for $\mu = 0$).

The relative sizes of S_0 and $\varphi(S_0)$ will depend on λ_1, λ_2 and on our choices of h, k, ε_1, ε_2 and $\bar{r}_2$. We have so far left these open, though for later parts of the analysis

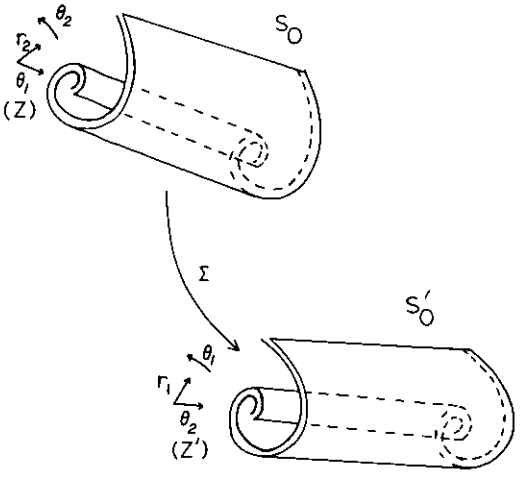

Figure 3. The set S_0 in B given by (2.7) is a thick spiral, or scroll. Σ maps S_0 into another thick scroll S_0' interchanging the θ_1 and θ_2 directions.

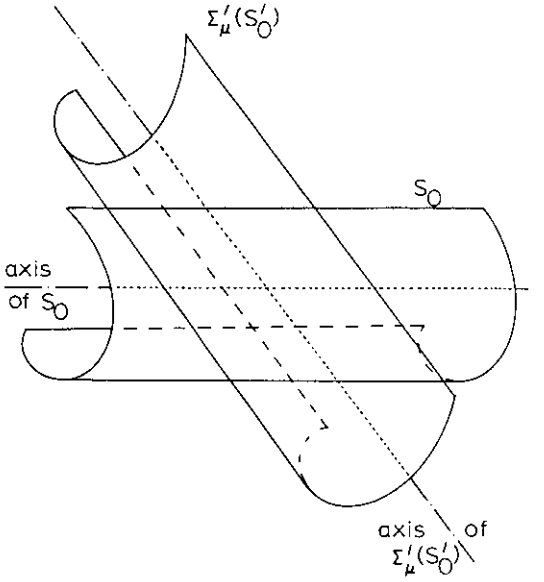

Figure 4. The scrolls S_0 and $\Sigma'_\mu(S'_0)$ in B. The axes of these scrolls are in general ($\mu \neq 0$) non-intersecting and skew.

it is helpful to make some definite choices. We already know that we want $\bar{r}_2 \ll h$, k. If we choose ε_2 so that S'_0 is approximately the same width ($k\varepsilon_2$) as it has radius ($\bar{r}_1$) we need to take $k\varepsilon_2 \approx \bar{r}_1$ which implies $\varepsilon_2 \approx (h/k)(\bar{r}_2/k)^\delta$ where $\delta = \lambda_1/\lambda_2$. Then, if elements of A are of size $|A|$ (this could be an appropriate norm of A, for example) we may expect from (2.6) that the image of S' under Σ'_μ has size $|A|h(\bar{r}_2/k)^\delta$ $(+O(\mu))$ and that, therefore, points in $\Sigma'_\mu(S'_0) = \varphi(S_0)$ have

$$\begin{aligned} r_2^1 &\sim |A|\, h(\bar{r}_2/k)^\delta (+O(\mu)) \\ \theta_1^2 &\sim |A|\, (\bar{r}_2/k)^\delta. \end{aligned} \tag{2.10}$$

Consideration of $r_1 r_2^\delta$—which is constant near 0—suggests that in fact $|A| \sim k^\delta h^{-1/\delta}$, which is invariant under time reversal ($|A| \to |A|^{-1}$, $\delta \to \delta^{-1}$, $h \to k$) as it should be. Substituting into (2.10) gives us

$$\begin{aligned} r_2^1 &\sim h^{1-1/\delta} \bar{r}_2^\delta + O(\mu) \\ \theta_1^1 &\sim h^{-1/\delta} \bar{r}_2^\delta \end{aligned} \tag{2.11}$$

in S, so that the size of $\varphi(S_0)$ is independent of k (as it should be), and also that $r_2^1 h^{1/\delta}$ is independent of h (as it should be). The expressions (2.11) also suggest that we consider the appropriate part of S if we take $\varepsilon_1 \approx h^{1/\delta} \bar{r}_2^\delta$, which we therefore do.

For fixed h and k, then, we start with a set S_0 of width $\sim \bar{r}_2^\delta$ and radius $\sim \bar{r}_2$. This maps by Σ into a set S'_0 of width and radius $\sim \bar{r}_2^\delta$ which is mapped by Σ'_μ back into a set $\varphi(S_0)$ of approximately the same size ($\bar{r}_2^\delta$). The image of S_0 under φ is therefore of approximately the same width as S_0 (by choice), but its radius, $\bar{r}_2^\delta$, is larger than the radius of $S_0(\bar{r}_2)$ if $\lambda_1 < \lambda_2$ (expansion stronger than contraction) or smaller if $\lambda_1 > \lambda_2$ (contraction stronger than expansion). Other choices of the variables could have been made (for instance, to make S_0 of roughly equal radius and width) but wherever necessary we will use those above. We retain both h and k (rather than

fixing one in terms of the other) since this makes it slightly more obvious how one formula depends on another.

It is clear that if S_0 contains an invariant set—that is, a set Λ which satisfies $\varphi(\Lambda) = \Lambda$ and such that points in Λ continually return to S_0 under application of φ (and φ^{-1})—then this set must be a subset of the intersection $S_1 = S_0 \cap \varphi(S_0)$. The rest of this paper concerns the geometry and dynamics of the components of S_1.

3. The geometry of S_1: intersecting skewed spiral sheets

In this section, we will present a variety of ways of understanding what the intersection $S_1 = S_0 \cap \varphi(S_0)$ looks like, and how its components change as μ changes. In the general (skewed) case, S_1 is a nearly one-dimensional structure consisting of a number of disconnected 'thick' curves or *cords*. We will begin by studying the one-dimensional structure, and to this end, we consider S_0 and $\varphi(S_0) = T_0$ as being represented by two spiral sheets, or scrolls, of two dimensions. These can be specifically defined using (2.7) and (2.8):

$$\begin{aligned} &S_0 : r_2 \leqslant \bar{r}_2 \qquad |\theta_1| \leqslant \delta_1 \qquad \theta_2 + \frac{\omega_2}{\lambda_2}\ln(k/r_2) = 0 \\ &S_0' : r_1 \leqslant \bar{r}_1 \qquad |\theta_2| \leqslant \delta_2 \qquad \theta_1 - \frac{\omega_1}{\lambda_1}\ln(h/r_1) = 0 \\ &T_0 : \Sigma_\mu'(S_0'). \end{aligned} \tag{3.1}$$

In order to describe what the components of S_1 are like, we can make use of a diagram like that in figure 5. We call one (either) scroll the vertical (V) scroll, and call the other the horizontal (H) scroll. (Our arguments will work whenever the axes of S_0 and T_0 are not parallel, which is generally the case.) We choose a section Π through the H scroll which includes its axis. The sheets of the scroll H then intersect Π in an infinite series of parallel lines, as shown in figure 5. The dotted spiral at the right of figure 5 indicates how the lines are joined by the sheets of H outside Π. We could label parts of H with integers, H_0, H_1, etc., each integer representing a

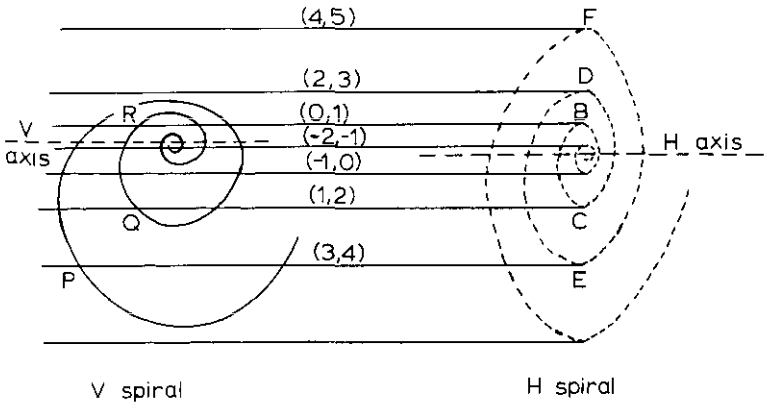

Figure 5. The plane Π, showing intersections with the H-scroll and V-scroll. The labelling is explained in the text.

connected piece of H above or below Π on which the angle variable varies by π. The lines are designated by pairs of integers $(4, 5)$, $(2, 3)$ etc, showing which two pieces of H join at this line. (The series of integers is, of course, infinite, with infinitely many lines $(-n, -n+1)$, converging on the axis.) The vertical scroll V intersects Π as shown in solid lines at the left of figure 5.

To describe components of S_1, we merely have to choose a point on $H \cap V$, and to track it as its radius on H varies, so that the corresponding radius in V varies continuously.

To illustrate, consider the intersection of the scrolls near the V-axis. The V-axis intersects many different sheets of H. For example, the intersection of V with sheet $H_4(EF)$ of H gives the following. For points near the V-axis, the sheet H_4 (i.e. EF) is almost planar, and the intersection of V with H_4 gives an S_1 component which is essentially a spiral which winds out from the V-axis on H_4. As it winds out further and further, it oscillates more and more on H_4, and this continues until it runs out of H_4. This is when it reaches the point P on V, E on H. At this point, the S_1 component is parallel to the V axis. A little thought shows that the continuation of the component moves past E on H to sheet $H_3(ED)$ on H, whereas the component reverses direction on V at P, and starts to wind back in towards the V axis. It continues to do this, winding inwards on V, and oscillating decreasingly on H_3 until it finally asymptotes to the V axis. Notice that this is able to happen because the component never reaches D on H_3.

We term such a component a *homo-axial* spiral. It winds out from the V-axis on sheet H_4, moves over to H_3, and winds back in towards the V-axis on H_3. A schematic representation of a homo-axial spiral is shown in figure 6.

Now look at the intersection of the V-axis with sheet H_2 of $H(CD)$. As before, a spiral winds out from the V-axis while the component oscillates back and forth on H_2. The first crisis occurs at C on H_2, and Q on V. Here the component reverses direction on V, and moves on to sheet H_1. Now, however, as the component winds inwards on V, it suffers another crisis at B in H, reverses direction at R on V, and continues on to sheet H_0. Evidently it continues to shuttle back and forth on that part of V between Q and R, and winds in towards the H-axis. We term this a *hetero-axial* spiral. A view is shown in figure 7.

There also exist closed *loops*. An example is shown in figure 8. A loop exists on sheets V_2 and V_3, and on sheets H_1 and H_2 between the lines $H(1, 2)$ and $V(2, 3)$. The loop goes from points AB' to BA' to CB' to BC' and back to AB'.

The notation for the H lines (which we shall call axial lines) gives an easy method for following components of S_1. Starting from any point in S_1 (on H and V at the same ordinate in figure 5) we wind round V on sheet H_i (say) till we get to an H-line with an i in it—either $H(i, i+1)$ or $H(i-1, i)$; at this point we reverse direction in V and move to H_{i+1} or H_{i-1} as appropriate. (This prescription is

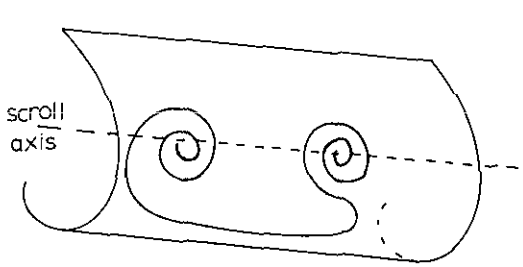

Figure 6. A homo-axial spiral.

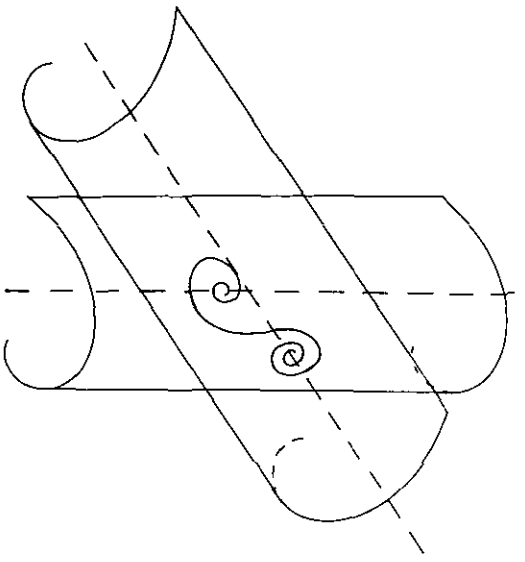

Figure 7. A hetero-axial spiral.

sufficient, but it sometimes suits us for descriptive purposes, as in the description of figure 8, to introduce the obvious notation for V sheets and V axial lines as well.)

The three types of constituents described above are the only possible types of component in S_1. What we now wish to do is to understand how these constituents arise and how they bifurcate amongst themselves as μ changes.

3.1. Bifurcation of geometry: unrolled scrolls

Let us now consider how the homo-axial and hetero-axial spirals, and closed loops, are generated as the parameter μ is changed. As we decrease μ towards zero, we can suppose that the V spiral approaches the H axis, as shown in figure 9. The first thing that happens, as a sheet of V crosses one of the axial lines of H, is that a small closed loop is created. This has just happened on $H(1, 2)$ in figure 9(a). As μ decreases, V descends to position (b) in figure 9. The loop expands on sheets 1 and 2 of H. Further loops are created as further sheets of V cross $H(1, 2)$. Nothing happens to these loops (other than becoming larger) as μ decreases until the V sheet on which the large loop exists crosses the line $H(0, 1)$, as in figure 9(d). When this happens, appeal to the recipe given above shows that a bifurcation occurs. The (large) closed loop no longer exists, and this component of S_1 is now part of a homo-axial (H) spiral. Just before the bifurcation, figure 9(c), there is the closed

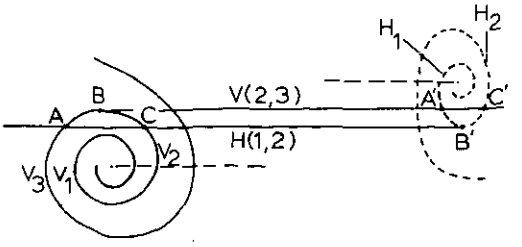

Figure 8. Existence of closed loops.

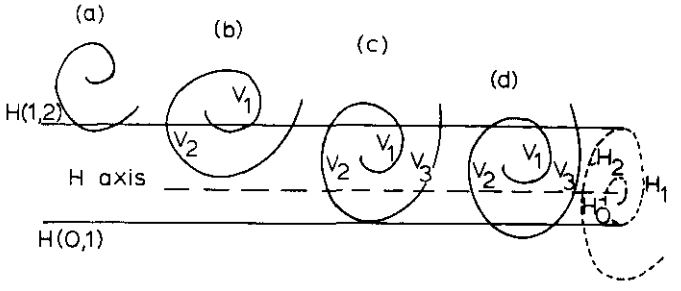

Figure 9. μ decreases towards zero as V goes from (a) to (d).

loop on sheets H_1 and H_2 and V_2 and V_3. In addition, there is a homo-axial H spiral on sheets V_2 and V_3. which reaches H_0. It is easy to see that this homo-axial is created just after figure 9(b), when the axial line $V(1, 2)$ crosses the H axis. Just after the bifurcation, in figure 9(d), this homo-axial winds on to sheets H_1 and H_2, where it then crosses to sheet V_3 and winds back to the H axis. This extra excursion on H_1, H_2 consumes the loop which previously existed on sheets H_1 and H_2.

A less wordy and more comprehensible way of visualizing this bifurcation is to unroll the H scroll, so that it lies flat. The appropriate diagram is then figure 10. the H axis is at $-\infty$ in this picture, the sheets H_1, H_2 etc lie next to each other, separated by the axial lines $H(0, 1)$, $H(1, 2)$, etc. The diagram depicts in heavy lines the situation in figure 9(c). Loops are created on the line $(1, 2)$ as μ decreases. When the loop reaches the line $(0, 1)$ on H, a bifurcation occurs, in which the pre-existing loop joins to a homo-axial H spiral, to form a larger homo-axial H spiral, as indicated by the dotted lines in figure 10. Thus, we have the bifurcation scheme

(A) homo-axial + loop→ homo-axial.

Evidently, the homo-axials are generated at the left (by the intersection of V sheets with H axis) and move to the right by consuming loops in the manner just discussed.

Exactly the same process occurs for homo-axial V spirals. As the V axis nears an axial H line, infinitely many loops are generated at a 'centre' (on the unrolled H scroll). When the V axis crosses the H line, a homo-axial V spiral is produced, which proceeds to consume the previously produced loops from the *inside* (as seen on the H scroll). This scheme of affairs is represented in figure 11.

It is fairly obvious how to elucidate what happens when homo-axial V spirals approach the H axial lines. The possibilities are sketched in figures 12 and 13. In figure 12, we see a bifurcation involving two homo-axial spirals: the scheme is

(B) H homo-axial + V homo-axial→ 2 hetero-axials.

This provides a mechanism for generation of hetero-axial spirals. Figure 13 shows the bifurcation of a hetero-axial with a homo-axial. The scheme is

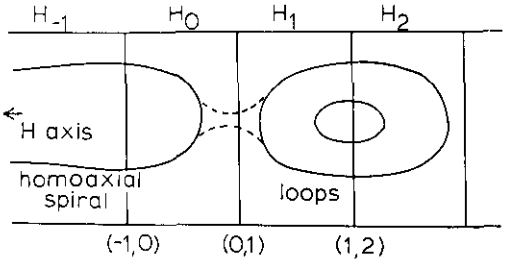

Figure 10. Unrolled H scroll; a type A bifurcation.

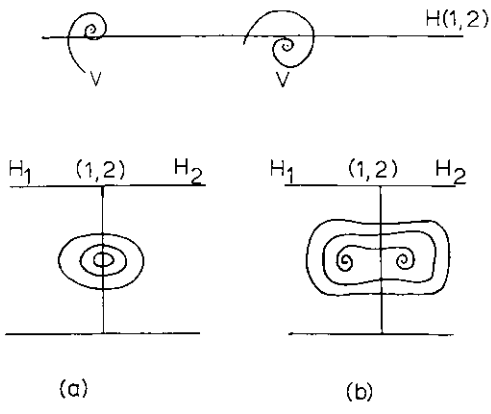

Figure 11. Generation and destruction of loops by a homo-axial V spiral, as depicted on an unrolled H scroll; a type A bifurcation.

(C) hetero-axial + V homo-axial → hetero-axial + V homo-axial.

This scheme propagates hetero-axials to the right, and homo-axials to the left.

In summary, consideration of an unrolled (H) scroll indicates the following sequence as μ is decreased.

(i) Loops are generated on axial H lines at the right, appearing further to the left as μ decreases.

(ii) H homo-axials are generated at the left, and propagate to the right by consuming the loops produced in (i) (type A bifurcation).

(iii) V homo-axials are generated at the right, and also consume loops produced in (i) (type A bifurcation).

(iv) H and V homoaxials interact via type (B) bifurcations (figure 12) to generate heteroaxials.

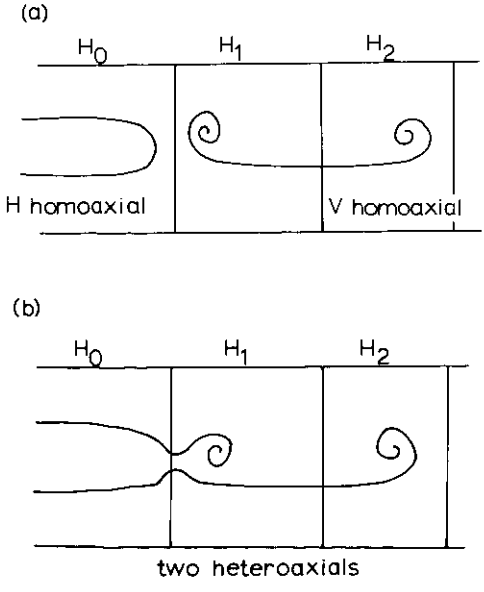

Figure 12. A type B bifurcation; H and V homo-axials meet to form two hetero-axial spirals.

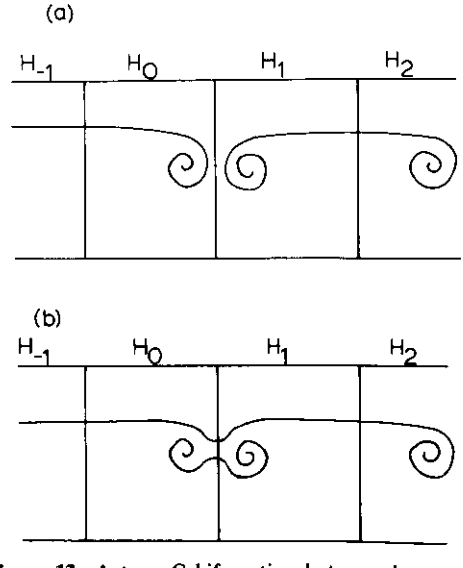

Figure 13. A type C bifurcation between hetero-axial and homo-axial spirals.

(v) Hetero-axials propagate to the right, and V homo-axials to the left, via type (C) bifurcations, as in figure 13.

This is all the bifurcation of the topology of S_1 which occurs as μ varies. Its symmetric counterpart occurs as μ decreases below zero and the V spiral leaves the vicinity of the H spiral.

3.2. A method of drawing S_1, symmetric between H and V scrolls

The disadvantage of the method of seeing the geometry and bifurcation of S_1 that we have just described, is its lack of symmetry between the H and V scrolls. (One of its advantages was the ease of visualization.) We now introduce a method which has this symmetry.

We first notice that a point Q on the H scroll has a certain radius r_H (distance from the H-axis), and if it also lies on the V scroll it also has a V-radius r_V (distance from the V axis). The set of points in H with H-radius r_H forms a line parallel to the H-axis and, similarly, the set of points with V-radius r_V forms a line parallel to the V-axis. These two lines intersect at Q, but nowhere else. Hence we can uniquely identify Q by writing down the pair of radii (r_H, r_V). We can similarly identify all points in S_1, and plot them on a diagram showing r_H against r_V. Figure 14 shows several such diagrams.

Returning now to consideration of the scrolls S_0 and T_0 given by equations (3.1), let us suppose that the H scroll is S_0 and the V scroll is T_0. We are free, if we like, to use the coordinates from S_0' in our description of T_0 (the mapping Σ' is affine and so well behaved) and so r_H is measured uniquely by r_2 and r_V by r_1. The condition that some pair of values (r_2, r_1) represents a point in S_1, the intersection of S_0 and T_0, can now be calculated.

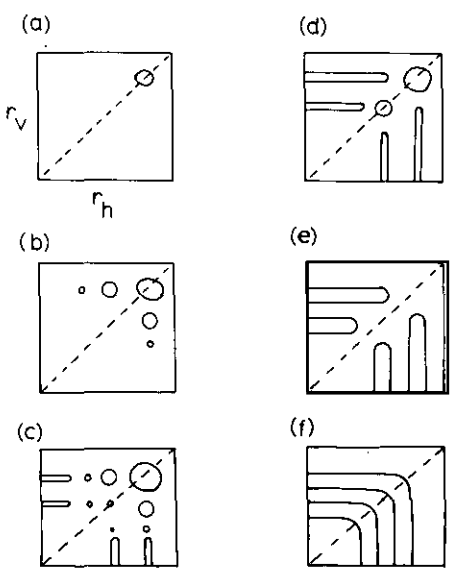

Figure 14. Evolution of S_1 in the (r_H, r_V) plane as μ changes. The sequence evolves as in the description in section 3. First, loops are generated at fixed points $(r_H = r_V)$. These propagate towards the axes. In (c), homo-axial spirals are generated; these propagate towards $r_H = r_V$ by consuming loops in bifurcations of type A. In (e), approaching homo-axials lead to type B bifurcations, forming hetero-axials in (f). Type C bifurcations merely rearrange the spirals, and are not shown. As μ changes further, the above sequence is reversed.

In (X, Y, Z) coordinates, the line of points in S_0 with radius r_2 is given by

$$\begin{aligned} X &= r_2 \cos\theta_2 \\ Y &= r_2 \sin\theta_2 \\ Z &\text{ arbitrary} \end{aligned} \tag{3.2}$$

and, from (3.1),

$$\theta_2 + \frac{\omega_2}{\lambda_2}\ln(k/r_2) = 0. \tag{3.3}$$

Similarly, in S_0', the (X', Y', Z') coordinates of the line of points with radius r_1 is given by

$$\begin{aligned} X' &= r_1 \cos\theta_1 \\ Y' &= r_1 \sin\theta_1 \\ Z' &\text{ arbitrary} \end{aligned} \tag{3.4}$$

where (3.1) tells us

$$\theta_1 - \frac{\omega_1}{\lambda_1}\ln(h/r_1) = 0. \tag{3.5}$$

Under Σ_μ', the line given by (3.4) is mapped, according to equation (2.6), to

$$\begin{pmatrix} X \\ Y \\ Z \end{pmatrix} = A\begin{pmatrix} r_1\cos\theta_1 \\ r_1\sin\theta_1 \\ Z' \end{pmatrix} + \mathbf{d}\mu \tag{3.6}$$

so writing A out in full as (a_{ij}), $1 \leqslant i, j \leqslant 3$, we find that the two lines (3.2) and (3.4) intersect if and only if we can find X and Y (with Z' arbitrary) satisfying:

$$\begin{aligned} X = r_2\cos\theta_2 &= a_{11}r_1\cos\theta_1 + a_{12}r_1\sin\theta_1 + a_{13}Z' + d_1\mu \\ Y = r_2\sin\theta_2 &= a_{21}r_1\cos\theta_1 + a_{22}r_1\sin\theta_1 + a_{23}Z' + d_2\mu \end{aligned} \tag{3.7}$$

where θ_2 and θ_1 are given by (3.3) and (3.5) above. Eliminating Z', and introducing new constants α, φ_1, φ_2, d, we can write (3.7) in the form

$$r_2\cos(\theta_2 + \varphi_2) = \alpha r_1\cos(\theta_1 + \varphi_1) + \mu$$

where we have rescaled μ, or, substituting in from (3.3) to (3.5),

$$r_2\cos\left(-\frac{\omega_2}{\lambda_2}\ln(k/r_2) + \varphi_2\right) = \alpha r_1\cos\left(\frac{\omega_1}{\lambda_1}\ln(h/r_1) + \varphi_1\right) + \mu. \tag{3.8}$$

Solutions of this equation, for various values of the constants and of μ, look like the diagrams plotted in figure 14, as can be easily checked.

4. A multi-valued one-dimensional map to model φ

Our aim in this section is to consider the full three-dimensional return map $\varphi = \Sigma_\mu'\Sigma$ and to derive a multi-valued one-dimensional map Φ_μ which will model forward

orbits of φ that remain in S_0 for ever. We will obtain such a map in the form

$$L(r_2^{i+1}) = R_\mu(r_2^i) \tag{4.1}$$

where L and R_μ are both functions defined in $r_2^i \leqslant \bar{r}_2$. Given a sequence of points $x^i = (r_2^i, \theta_1^i, \theta_2^i)$ generated by φ, so that $x^{i+1} = \varphi(x^i)$, $x^i \in S_0 \, \forall i \geqslant 0$, we will show that the successive r_2-values, r_2^i, approximately satisfy (4.1). Conversely, we will argue that most finite sequences of r_2-values $(r_2^0, r_2^1, \ldots)$ satisfying (4.1) can be well approximated by the sequence of r_2-values achieved by an orbit $\varphi^i(y)$ for some points $y \in S_0$. Thus, we will be able to study the maps (4.1) to obtain information about the behaviour likely to be observed in examples of differential equations having a homoclinic orbit of the kind discussed here.

It is possible to derive an approximate formula for functions L and R_μ satisfied by iterates $x^{i+1} = \varphi(x^i)$ by combining equations (2.4) and (2.6) to generate φ and using equation (2.7) to ensure that both x^i and x^{i+1} lie in S_0. The answer so obtained is

$$r_2^{i+1} \cos\left(-\frac{\omega_2}{\lambda_2} \ln(k/r_2^{i+1}) + \varphi_2 \right) = \beta (r_2^i)^\delta \cos\left(\frac{\omega_1}{\lambda_2} \ln(k/r_2^i) + \varphi_1 \right) + \mu. \tag{4.2}$$

which is of the form advertised in equation (4.1). However, this calculation largely mimics the calculation of the equation (3.8) in the last section, and it is more instructive to derive (4.2) directly from (3.8) since this involves us in a geometric argument about the way in which φ acts on S_0. This argument will give us, at the same time, the result about the existence of trajectories approximating sequences generated with equation (4.2).

Let us consider a point $x^i = (r_2^i, \theta_1^i, \theta_2^i)$ in one component of S_1. Recall that S_0 and S_0' are actually three-dimensional (and that we are describing their extent in the Z,Z' directions as *width*). Our point x^i will be close to a point y in one of the one-dimensional components of the approximation to S_1, which we discussed in the last section. We now consider a segment of the three-dimensional cord in S_1 which contains x^i and y, and which corresponds to a small piece of the one-dimensional approximation to S_1. Its length is the length of this one-dimensional approximation, while its thickness will be that of S_0 (in the radial direction) and its width (in S_0) will be the thickness of T_0.

In particular, the segment samples all values of θ_2 allowed by equation (2.7) but only a small fraction of the θ_1 values. The image under Σ of this segment in S_0' will, therefore, do a similar thing; it will sample the complete range of θ_2 values allowed by equation (2.8), but only a small fraction of the θ_1 values. In other words, the image in S_0' is a very thin ribbon stretching across the whole width (in the Z' direction) of S_0'. When mapped by Σ_μ' into $T = \varphi(S_0)$, this ribbon will intersect all components of S_1 that extend to the appropriate r_1-radius in the sense used in section 3.

To be more specific, if we use the sizes mentioned at the end of section 2, and we begin with a segment at almost constant radius r_2^i in S_0, it will have actual thickness $r_2^i \varepsilon_2$ and width less than or equal to $\varepsilon_1^2 h$ (depending on the r_1-value of the segment). This will be mapped to a thin ribbon in S_0' at almost constant radius $r_1^i = h[r_2^i/k]^\delta$ where $\delta = \lambda_1/\lambda_2$ (see equation (2.4)), of thickness $\varepsilon_1^2 r_1^i$ (compared with a thickness of $\varepsilon_1 r_1^i$ for the scroll S_0') and width equal to the whole width of S_0'. Under Σ_μ' this ribbon will once again intersect S_0 in small segments that typically sample the whole

thickness of S_0 but have width only $\varepsilon_1^3 h$ (or less). The places where the ribbon (which had r_1-value r_1^i in S_0') intersects S_1 will be close to points on the one-dimensional approximation of S_1 with description (r_2^{i+1}, r_1^i) in the notation of section 3, and where we must, therefore, have r_2^{i+1} and r_1^i satisfying equation (3.8). The fact that the ribbon stretches the whole width of S_0' implies that the image of our original segment under φ will intersect S_1 near to all such points, and the image of x^i will lie close to one of them since x^{i+1} is also in S_1 (by assumption).

Now, if we combine equation (3.8) with $r_1^i = h[r_2^i/k]^\delta$, we do indeed obtain equation (4.2) after introducing the new constant $\beta = \alpha h k^{-\delta}$. Thus (a) we have shown that (4.2) is approximately satisfied for points in S_1, and (b) we have a strong argument that near to a point x^i with radius r_2^i in S_1 we will be able to find points y such that $\varphi(y)$ has any r_2-value r_2^{i+1} satisfying (4.2).

The argument for (b) requires that the intersection of S_0 and T_0 be transverse near x^i. In particular, it will not work if S_0 and T_0 intersect in such a way that the component of S_1 containing x^i does not sample the full thickness of S_0. We will not pursue this possibility since it is evident that for most finite sequences of iterates it will not occur. Notice, however, that if we restrict our attention to parts of S_1 where the intersection is transversal, we can generate, in a standard way, a nested sequence of sets $S_i = \varphi(S_{i-1}) \cap S_0$ of width $\varepsilon_1^i h$ in S_0. These will converge to some Cantor set of ribbons, $S_\infty \subset S_1$, and if we label the components of S_1 with integers we will be able to construct the usual kinds of symbolic dynamics and will be close to recovering Shil'nikov's results about the existence of infinitely many periodic orbits and aperiodic trajectories in the flow.

It remains for us to describe how to use equation (4.2) before continuing, in the next section, to examine some of its behaviour and bifurcations. We shall describe two methods, one related to the way of looking at S_1 illustrated in figures 8 and 9, and the other related to the way of looking at S_1 illustrated in figure 14.

Figure 15 shows the two functions $L(r)$ and $R_\mu(r)$ superimposed on a diagram like figures 5 and 8. The relationship between the functions and the scrolls is apparent. The lower curve is $y = R_\mu(r)$, the upper is $y = L(r)$. For a given r-value, say r_2^i, we find the following iterate by following the vertical line $r = r_2^i$ until we reach the y value given by $y_1 = R_\mu(r_2^i)$. The possible value(s) of r_2^{i+1} are those for

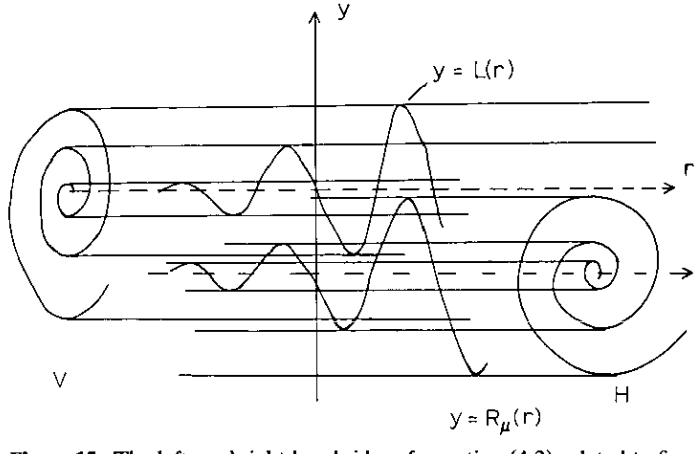

Figure 15. The left- and right-hand sides of equation (4.2) related to figures like figure 8

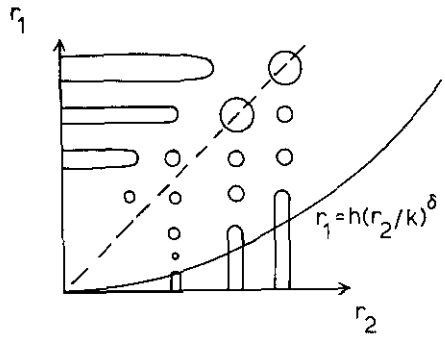

Figure 16. Plotting iterates of (4.2) on an (r_2, r_1) plot of S_1 like figure 14. The graph superimposed on the plot is $r_1 = h(r_2/k)^\delta$, illustrated here for $\delta = \lambda_1/\lambda_2 > 1$.

which $L(r_2^{i+1}) = y_1$, and these are those values of r at which the horizontal line $y = y_1$ intersects $y = L(r)$. It is evident that there are generally a number of possible values of r_2^{i+1}.

The other technique is illustrated in figure 16. Here we have plotted the curve $r_1 = h(r_2/k)^\delta$ on top of an (r_1, r_2) plot like those in figure 14. (We have chosen to illustrate the case $\delta = \lambda_1/\lambda_2 > 1$.) Now, given an initial value r_2^0, we move vertically to the curve $r_1 = h(r_2^0/k)^\delta$ to obtain the appropriate r_1 value. We then move horizontally to any point on a component of S_1 so that the new r_2^1 and $h(r_2^0/k)^\delta$ satisfy, respectively, the left- and right-hand sides of equation (3.8). This is equivalent to r_2^1 and r_2^0 satisfying the left- and right-hand sides of equation (4.2). To generate further iterates we continue to alternately move vertically to the graph and horizontally to any component of S_1.

5. Bifurcation of orbits

Fixed points of the map described in the last section will correspond to fixed points of the mapping φ, and these in turn correspond to periodic orbits of the flow which pass only once through S_0 before joining up. Thus, it is apparent that we can learn a lot about the existence and bifurcation of periodic orbits in the flow by looking at the fixed points of maps such as that shown in figure 16. Let us first consider the situation when $\mu = 0$.

When $\mu = 0$, the axes of the two scrolls intersect at P and it is clear that there will be infinitely many components of the one-dimensional representation of the set S_1 accumulating on $r_2 = r_1 = 0$. (The axis of each scroll intersects infinitely many sheets of the other scroll.)

Figure 17 shows this situation for the two cases $\delta = \lambda_1/\lambda_2 > 1$ and $\delta < 1$. The only difference between these figures is the position of the graph $r_1 = h(r_2^0/k)^\delta$; in both figures there are infinitely many fixed points of the mapping given by intersections of the graph with the one-dimensional (r_2, r_1) representation of the set S_1. These intersections accumulate along one axis or the other (depending on $\delta > 1$ or $\delta < 1$) and we can calculate the asymptotic period of the orbits (in the flow) represented by these intersections. From section 2 we find that the time spent between the surfaces S and S' is $\sim(1/\lambda_2)\ln[k/r]$, where r is the value of r_2 in S (at a fixed point of φ). Since most of the orbit's period is spent near the origin, this is the asymptotic value of the period, except that P cannot depend on k, which merely locates the box S'. We deduce that the time spent by the orbit between S' and S is $\ln(1/k) + O(1)$, and

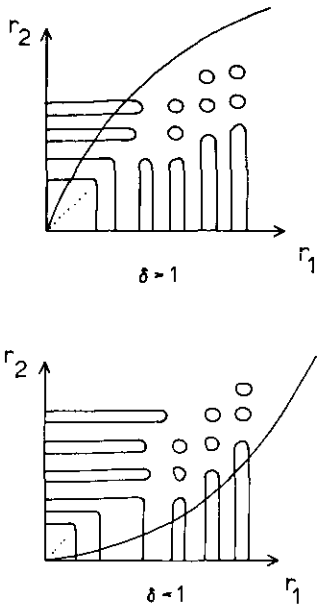

Figure 17. Infinitely many fixed points of the mapping for $\mu = 0$ accumulate along the r_2-axis of $\delta > 1$ and along the r_1-axis if $\delta < 1$.

that the period P is related to μ and r by

$$P \sim \frac{1}{\lambda_2} \ln(1/r). \tag{5.1}$$

Defining P_n to be the period of the orbit represented by the nth intersection (starting at some convenient place and counting upwards as the r_2-value at the intersection tends to zero) we can see that in the asymptotic regime we will have (using equations (3.8) and (5.1))

$$\text{If } \delta > 1;\ P_n \sim n\pi/|\omega_2| \tag{5.2a}$$

$$\text{If } \delta < 1;\ P_n \sim n\pi/|\omega_1|. \tag{5.2b}$$

In fact, if we are now prepared to vary μ we can, given a period P, determine an associated r_2-radius $r_2 \sim e^{-\lambda_2 P}$ and can, using equation (3.8) or (4.2) obtain the relationships

$$\delta > 1;\ \mu \propto e^{-\lambda_2 P} \cos[\omega_2 P + O(1)] \tag{5.3a}$$

$$\delta < 1;\ \mu \propto e^{-\lambda_1 P} \cos[\omega_1 P + O(1)] \tag{5.3b}$$

for μ-values at which periodic orbits of period P exist as $P \to \infty$. Figure 18 shows a bifurcation diagram of period against μ for orbits represented by fixed points of our one-dimensional map. Equations (5.3) show that the wiggles in figure 18 will decrease in size very rapidly as $P \to \infty$ if $\lambda_i \pi/|\omega_i|$ is large for the relevant index $i = 1$ or 2.

Notice that figure 18 is consistent with our knowledge that there are infinitely many periodic orbits when $\mu = 0$; it is just that we have joined them together into a single family which can be traced by increasing and decreasing μ whilst increasing P monotonically. If we are obliged to increase μ monotonically we will see only that pairs of orbits appear or disappear in saddle-node bifurcations at the points where the curve in figure 18 is vertical. Figure 19 shows a sequence of bifurcations as μ

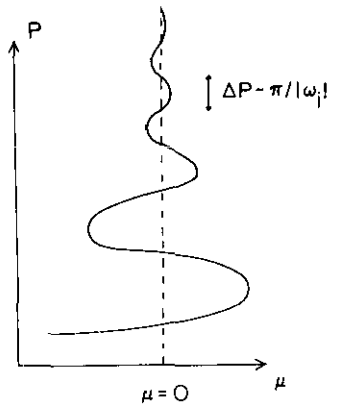

Figure 18. μ against period P for the periodic orbits represented by fixed points of the one-dimensional map.

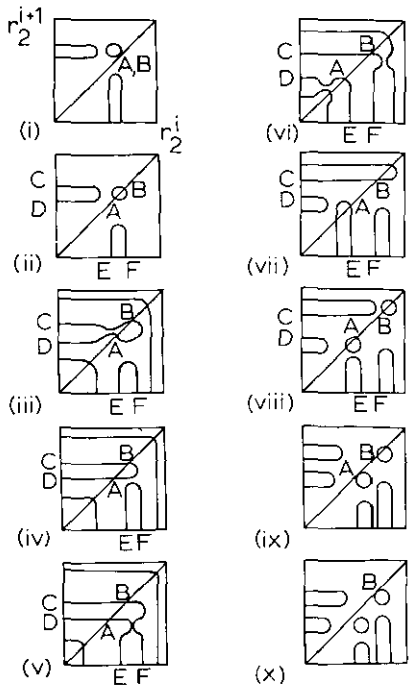

Figure 19. *Details of bifurcations between loops* and spirals as μ changes monotonically. Two fixed points, A and B, produced in a saddle-node bifurcation in frame (i) are eventually destroyed in separate bifurcations in frames (ix) and (x). Here we show the bifurcations on an (r_2^i, r_2^{i+1}) plot (see (4.2)), which is topologically equivalent to the (r_2, r_1) plot of figure 16 (see (3.8)).

varies monotonically (from positive to negative, say) following two fixed points, A and B, from their appearance in one saddle-node bifurcation to their separate destruction in two other similar bifurcations. Just as the two points A and B move onto different loops at some point in this sequence, so the points C and D, and E and F, get separated from one another on the components of S_1 representing homo-axials; a little thought about the geometry of the scrolls leads one to the conclusion that this is exactly what we would expect to happen to homo-axial components as one scroll moves through the other. Now, while increasing μ again from the value shown in the last frame of figure 19, we can follow the other fixed point (besides A) involved in the saddle-node bifurcation of that frame through a similar sequence of changes, and eventually, moving μ up and down through zero can follow the fixed point continuously down towards $r_1 = r_2 = 0$. This process is the precise counterpart of following the curve of figure 18 as $P \to \infty$.

Figure 18 is the basis of our assertion that for large enough μ values it is likely that the effect of all the complicated bifurcations close to $\mu = 0$ is just to produce a single periodic orbit. This orbit is the continuation of the curve shown in figure 18 into parameter regions where there is no hope of justifying our analysis rigorously, and it could exist in either $\mu < 0$ or $\mu > 0$.

This argument is similar to one expounded at greater length in Glendinning and

Sparrow (1984) in relation to three-dimensional saddle-focus homoclinic bifurcations. In that case, all examples studied behave as expected. In the present case we expect that observed behaviour will depend strongly on the ratios $\lambda_i\pi/|\omega_i|$. If these are large, it may be difficult to observe anything other than the single periodic orbit since the wiggles of figure 18 will be small.

5.1. Stability of orbits; period-doubling bifurcation

The three eigenvalues of the full three-dimensional return map φ are $O(\varepsilon_1) \ll 1$, $O(\varepsilon_1 h/\varepsilon_2 \bar{r}_2) \gg 1$ and $\approx R'/L'$ where R' and L' are the derivatives of the right- and left-hand sides of equation (4.2) and where the sizes of the other constants were discussed in section 2. All fixed points are therefore saddles, but the O(1) eigenvalue goes from >1 to <1 at the turning points of the curve in figure 18. When $R' > L'$, trajectories have two unstable Lyapunov components, a situation commonly referred to as 'hyperchaos' when it affects whole invariant sets. (Glendinning and Tresser (1985) discuss this phenomenon in systems related to those studied here.)

Period-doubling bifurcations will occur when $R'/L' = -1$ and to visualise this it is easiest to plot equation (4.2) directly on our (r_1, r_2) plots, as was done in figure 19. This only has the effect of rescaling the diagrams we have been using so far (based on equation (3.8)) so that the graph of $r_1 = h(r_2/k)^\delta$ becomes a straight diagonal. We have resisted this simplification earlier since it slightly obscures the dependence of the asymptotic behaviour on δ. $R'/L' = -1$ now just means that near the fixed point the (r_2, r_1) plot considered as a function of r_2 has slope -1. Figure 20 shows a sequence of bifurcations starting with a period-doubling bifurcation in which a period 2 orbit is produced from a fixed point. (Period 2 orbits of the map represent

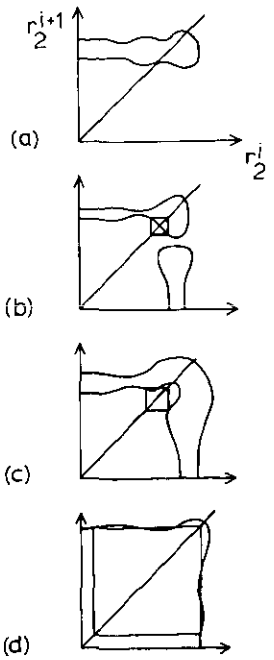

Figure 20. A fixed point period doubles (*a*)–(*b*) producing a periodic orbit of period 2. Following this orbit (by increasing and decreasing μ) it can be made to approach the axes (*d*).

periodic orbits of the flow which pass twice through the linear region near the bifocus before joining up.) In this case the period of the doubled orbit increases as it approaches the axes. It is, in fact, approaching a subsidiary homoclinic orbit.

5.2. Subsidiary homoclinic orbits

In addition to the homoclinic orbit which occurs at $\mu = 0$ (which we call the *primary* homoclinic orbit) we can expect other homoclinic orbits to exist for small μ-values. These are orbits which start on the unstable manifold of the fixed point in S_0' and which after a number of passages through S_0 and S_0' eventually land on the stable manifold of the fixed point in S_0. Following Glendinning and Sparrow (1984) we refer to such orbits as *subsidiary* homoclinic orbits, and Glendinning (1989) has shown that infinitely many such orbits do occur in a neighbourhood of $\mu = 0$. (The precise way in which their existence depends on μ is affected by the ratio of the angular frequencies ω_1 and ω_2.) In terms of our (r_2, r_1) plots, such an orbit occurs when a trajectory like that shown in figure 21 exists.

The full complexity of the bifurcation picture near $\mu = 0$ can be gathered from the fact that each of these homoclinic orbits can be analysed using the technique described in this paper, though the region of validity of the analysis will include only a very small subset of the μ- and r-values for which our analysis provides a good approximation to the behaviour. Nonetheless, we may deduce the existence of a global curve of periodic orbits like figure 18 for each of these homoclinic orbits, and figure 20 illustrated the way in which a period 2 orbit could increase in period by approaching one such homoclinic orbit in an appropriate way.

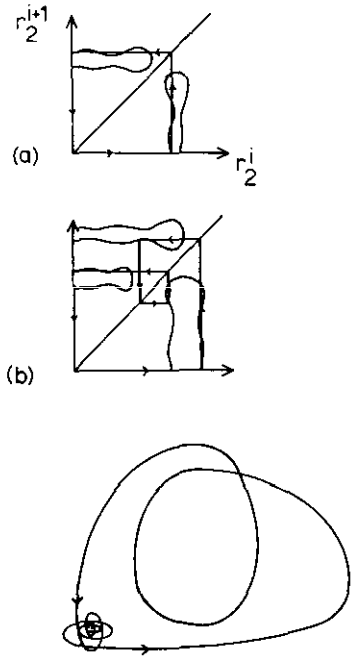

Figure 21. Subsidiary homoclinic orbits on (rescaled) (r_2, r_1) plots; (*a*) shows the simplest type where the orbit passes only once through the linear region near the bifocus; (*b*) shows a more complicated orbit; (*c*) illustrates the type of orbit associated with (*b*).

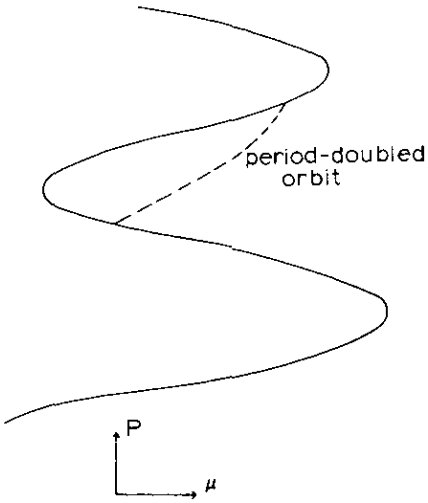

Figure 22. A period-doubled orbit is produced at one fixed point and destroyed at another distinct one.

5.3. Details of bifurcation structure

The bifurcations we have discussed so far differ little from those observed in three-dimensional systems with homoclinic orbits to saddle-focus (one real eigenvalue and one complex pair) fixed points. This is largely because if the ratio of exponents $\delta = \lambda_1/\lambda_2$ is not close to one, then the map (4.2) which really encapsulates the dynamics is close to that of the 3D saddle focus case. For example, if $\delta > 1$, then fixed points of (4.2) are given approximately by $L(r_2) = \mu$, which also approximately defines the map; this is similar to the three dimensional case. The real novelty of the bifocal example thus occurs when δ is close to one.

We have been unable to find an example on which to explore the bifocal distinctions. Nevertheless, it is possible to conjecture as to some behaviour which we might expect. In the three-dimensional (Shil'nikov) case, period-doubling bifurcations occur off the primary branch, and such period-doubled orbits may themselves become homoclinic, or rejoin the primary branch a little further up (or down), but without encountering a saddle node bifurcation. In the four-dimensional case, this is not necessarily true, and a period-doubled orbit may, in principle, rejoin the primary branch after a number of intervening saddle-node bifurcations. Such a possible situation is depicted in figure 22, where the period-doubled orbit rejoins the primary branch on a different arm, with a single saddle-node bifurcation in between.

6. Conclusion

We have described several powerful methods to visualize the geometry of the invariant set existing near a bifocal homoclinic orbit, and have derived a multivalued one-dimensional map with which the dynamics on the set can be approximated. These tools should considerably simplify the task of understanding bifurcation patterns occurring in examples. Our experience with the three-dimensional saddle-focus case suggests that the map and model described in this paper will prove

competent to predict results over large ranges of parameter values (much larger than can be expected on rigorous mathematical grounds). We can expect the details of fully fledged four-dimensional behaviour to be observed most easily in cases where $\lambda_1\pi/\omega_1$ and $\lambda_2\pi/\omega_2$ are of reasonable size and where λ_1 and λ_2 are of similar size.

Acknowledgments

We appreciate discussion with Alar Toomre, and also the hospitality of the GFD summer school at Woods Hole and its Director in 1984, Willem Malkus, where the brunt of this work was done. ACF gratefully acknowledges a research grant from the Research Corporation and CTS gratefully acknowledges a travel grant from the Royal Society and the King's College Research Centre.

References

Arneodo A, Coullet P and Tresser C 1982 Oscillators with chaotic behaviour: an illustration of a theorem by Shil'nikov *J. Stat. Phys.* **27** 171–82

Belitskii G R 1978 Equivalence and normal forms of germs of smooth mappings *Russ. Math. Surveys* **33** 107–77

Gaspard P 1984 Generation of a countable set of homoclinic flows through bifurcation in multi-dimensional systems *Bull. Class. Sci. Acad. R. Belg.* Serie 5 **LXX** 61–83

Glendinning P 1989 Subsidiary bifurcations near bifocal homoclinic orbits *Math. Proc. Camb. Phil. Soc.* **105** 597–605

Glendinning P and Sparrow C 1984 Local and global behaviour near homoclinic orbits *J. Stat. Phys.* **35** 645–96

Glendinning P and Tresser C 1985 Heteroclinic loops leading to hyperchaos *J. Physique Lett.* **46** L347–52

Guckenheimer J and Holmes P 1983 *Nonlinear oscillations, Dynamical Systems, and Bifurcations of Vector Fields* (Berlin: Springer)

Hartman P 1982 *Ordinary Differential Equations* 2nd edn (Basel: Birkhäuser)

Neimark J I and Shil'nikov L P 1965 A case of generation of periodic motions *Sov. Math. Dokl.* **6** 305–09

Shil'nikov L P 1965 A case of the existence of countable number of periodic motions *Sov. Math. Dokl.* **6** 163–66

—— 1967 The existence of a denumerable set of periodic motions in four-dimensional space in an extended neighbourhood of a saddle-focus *Sov. Math. Dokl.* **8** 54–8

—— 1968 On the generation of a periodic motion from trajectories doubly asymptotic to an equilibrium state of saddle type *Math. USSR Sb.* **6** 427–38

—— 1970 A contribution to the problem of the structure of an extended neighbourhood of a rough equilibrium state of saddle-focus type *Math. USSR Sb.* **10** 91–102

Sparrow, C 1982 The Lorenz equations: bifurcations, chaos, and strange attractors *Appl. Math. Sci.* **41** (Berlin: Springer)

Tresser C 1984 About some theorems by L P Shil'nikov, *Ann Inst. H. Poincaré* **40,** 441–61

Wiggins S 1988 Global bifurcations and chaos *Appl. Math. Sci.* **73** (Berlin: Springer)